

Measuring dynamic fast ion spatial profiles with fusion protons in the Madison Symmetric Torus

Cite as: Rev. Sci. Instrum. **89**, 101104 (2018); <https://doi.org/10.1063/1.5037349>

Submitted: 23 April 2018 . Accepted: 27 May 2018 . Published Online: 17 July 2018

R. M. Magee , J. K. Anderson , S. Korepanov, L. Frausto , J. Boguski, P. J. Bonofiglio , J. Kim, and R. McConnell



View Online



Export Citation



CrossMark

ARTICLES YOU MAY BE INTERESTED IN

[Measurement of electron temperature fluctuations on J-TEXT via correlation ECE](#)

Review of Scientific Instruments **89**, 10H105 (2018); <https://doi.org/10.1063/1.5035121>

[Development of an ordinary mode multi-channel correlation reflectometer on EAST tokamak](#)

Review of Scientific Instruments **89**, 10H103 (2018); <https://doi.org/10.1063/1.5035445>

[Scintillating fiber detectors for time evolution measurement of the triton burnup on the Large Helical Device](#)

Review of Scientific Instruments **89**, 10I105 (2018); <https://doi.org/10.1063/1.5035290>



JANIS

Rising LHe costs? Janis has a solution.
Janis' Recirculating Cryocooler eliminates the use of Liquid Helium for "wet" cryogenic systems.

sales@janis.com www.janis.com [Click for more information.](#)

Measuring dynamic fast ion spatial profiles with fusion protons in the Madison Symmetric Torus

R. M. Magee,^{1,a)} J. K. Anderson,² S. Korepanov,¹ L. Frausto,¹ J. Boguski,² P. J. Bonfiglio,² J. Kim,² and R. McConnell²

¹TAE Technologies, Inc., 19631 Pauling, Foothill Ranch, California 92610, USA

²University of Wisconsin–Madison, 1150 University Ave., Madison, Wisconsin 53706, USA

(Presented 18 April 2018; received 23 April 2018; accepted 27 May 2018; published online 17 July 2018)

Neutral beam injected fast ions play a dominant role in both the field reversed configuration (FRC) at TAE Technologies and the Madison Symmetric Torus (MST) reversed field pinch (RFP), making fast ion diagnosis a major pillar of both research programs. And as strongly self-organized plasmas, the FRC and RFP similarly exhibit dynamic relaxation events which can redistribute fast ions. Recently, a collaboration between TAE Technologies and the University of Wisconsin was conducted to develop a method for measuring a fast changing fast ion spatial profile with a fusion proton detector and to investigate commonalities between the two plasmas. The steerable detector was designed and built at TAE and installed on MST. The fusion proton emission profile resulting from injection of a 25 kV deuterium neutral beam is measured with better than 5 cm spatial resolution and 100 μ s temporal resolution over the course of several 10s of shots. The fast ion density profile, forward modeled by tracing the orbits of the 3 MeV protons through a reconstructed magnetic equilibrium, is observed to flatten during global magnetic tearing mode activity, dropping by 30% in the core and increasing by a similar amount at the edge. The equilibrium profile is observed to be consistent with measurements made with a collimated neutron detector. *Published by AIP Publishing.* <https://doi.org/10.1063/1.5037349>

I. INTRODUCTION

Minority populations of suprathermal ions, whether born from neutral beam injection (NBI), RF heating, or processes natural to the plasma (e.g., magnetic reconnection), often play an outsized role in plasma dynamics, so accurate diagnosis is critical.

Measurements of the flux of fusion products are ideal for fast ion diagnosis for a number of reasons: the sensitivity of the cross section to energy ensures that the signal is dominated by the highest energy ions; the emission does not require a high density of neutrals, so conditions in the hot core can be probed absent a neutral beam target; the particles are not confined by the magnetic field due to their high energy or, for the case of neutrons, lack of charge; and the detectors are passive and non-perturbative.

On the TAE field reversed configurations (FRCs) C-2U¹ and C-2W,² neutron and proton detectors are used in a complementary fashion. Calibrated, scintillator-based neutron detectors³ operated in current mode provide high time resolution, volume integrated measurements of the neutron flux from deuterium-deuterium fusion during deuterium NBI. The relatively low neutron flux (10^7 s⁻¹ cm²) precludes collimation, as has been done on other machines, so multiple, single-chord fusion proton detectors,⁴ operated in pulse-counting mode, are used to reconstruct the axial emission profile, as has been done in previous studies.^{5,6}

The focus of the present work is on the development of a steerable proton detector, capable of resolving the dynamic radial profile of the fusion proton emission from a single port. MST⁷ provides an ideal test bed for this diagnostic development: highly reproducible, fusion-grade plasmas at a high repetition rate (> 100 shots/day) and a high flux of NBI-induced deuterium fusion products (10^{10} s⁻¹ cm²; MST NBs operate at 25 keV, whereas C-2U/W NBs operate at 15 keV). Additionally, MST plasmas, like C-2U/W plasmas, exhibit fast, discrete relaxation events which redistribute fast ions, allowing us to simulate the FRC measurement in the RFP. Furthermore, both plasmas exhibit Alfvén and energetic particle mode activity, opening the possibility to studies of physics commonalities between the two devices.

II. HARDWARE

A. Detector

The detector is a large area (50 cm²), partially depleted Passivated Implanted Planar Silicon (PIPS) detector from Canberra Industries, Inc.⁸ The detector is negatively biased with 60-90 V, and the signal is amplified with a transimpedance amplifier with a gain of 10^6 V/A. Typical amplified signal pulses have a FWHM of 200 ns and an amplitude of 1 V. The signal is digitized at 60 MS/s. All pulse counting and pulse shape analysis is done digitally. The details of the electrical circuit are described in an earlier publication.⁴

B. Collimators

Detachable collimating heads are constructed by bundling small-diameter, seamless, smooth-bore stainless steel tubing in

Note: Paper published as part of the Proceedings of the 22nd Topical Conference on High-Temperature Plasma Diagnostics, San Diego, California, April 2018.

^{a)}Electronic mail: RMagee@TAE.com



FIG. 1. CAD renderings illustrate how the line of sight can be adjusted with a linear feedthrough without breaking vacuum. The collimation angle can be changed by swapping exchangeable collimators mounted to the end of the collimation tube (inset).

a 2" diameter sleeve, as illustrated in the inset of Fig. 1. The fine collimator (pictured left) is made up of approximately 200 tubes with 0.12" OD and 0.01" wall thickness cut to 3" lengths to give a collimation angle of 2°. The coarse collimator (pictured right) is made up of 10 tubes with 0.5" OD and 0.035" wall thickness cut to 2" in length for a collimation angle of 13°. The bundle is captured in the sleeve by slitting a 2" stainless steel tube, compressing the bundle, and tack welding the slit closed. It was discovered that due to the lack of compressibility of the small diameter tubes, it is necessary to insert a few larger diameter roll pins to prevent "rattlers"⁹ from coming dislodged.

The collimation tube is mounted on a hinge and articulated with a linear feedthrough to allow the line of sight to be changed continuously and without breaking vacuum, as illustrated in Fig. 1.

C. Foils

It is necessary to shield the detector from lower energy particles (e.g., fast charge-exchange neutrals) and soft x-rays. The limited thickness of the detector prevents very hard x-rays from being a concern as they mostly pass through the detector. The 300 μm silicon passes 150 keV x-rays with a transmission efficiency of 99%.¹⁰

A number of different foils were tested to find the optimum balance between passing fusion products and blocking x-rays and neutrals. We tested 800 nm Al, 40 μm Al, 5 μm Al/10 μm Pt, and 25 μm Al/20 μm Pt. The 800 nm foil was the most attractive at the outset, offering the possibility to collect not only the protons and tritons but also the ^3He particles, which originate from a different portion of the plasma as the other fusion products due to a smaller Larmor radius and thus providing an additional line of sight. Unfortunately, the x-ray transmissivity of this foil was too high and the detector signal experienced immediate hard saturation.

The optimum foil for the MST installation was found to be the combination of 5 μm Al and 10 μm Pt. (The purpose of the Al is to be a substrate for the Pt, which was available only in strips. The transmission of 10 μm Pt is substantially lower than 5 μm Al, so Al offers very little additional shielding.) This combination foil passes protons as well as 40 μm Al but is a better shield of x-rays due to the high-Z nature of the material, as illustrated in Fig. 2.

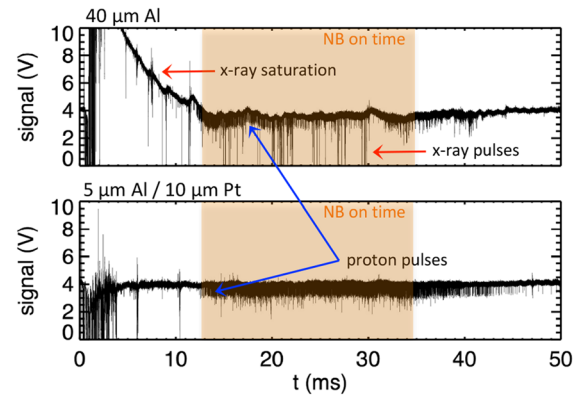


FIG. 2. A comparison of typical signals using a 40 μm Al foil (top frame) and a 5 μm Al/10 μm Pt combination foil (bottom frame). The early-in-time ($t < 10$ ms) saturation and the large spikes present in the top trace and absent in the bottom indicate that the 40 μm Al foil offers insufficient shielding of soft x-rays.

Runaway electrons in MST are the dominant source of soft x-rays,¹¹ but significant runaway populations have not been observed in C-2U or C-2W, so the x-ray environment is likely more forgiving and thin Al foils which pass the heavier fusion products may be workable in future TAE installations.

III. PULSE COUNTING

Pulse discrimination and counting is done digitally in post-shot processing. Discrimination by shape allows us to filter out electromagnetic pick-up and the small number of x-rays that penetrate the foil but are stopped in the silicon. Inspection of the raw signal reveals that most pulses are very similar in both shape and amplitude, so we assume that most pulses are in fact from fusion proton hits. Rather than constructing an artificial function to approximate the pulse shape, we instead average together a large number of actual, measured pulses. This is performed by first collecting a large number of pulses and averaging them together. We then pass through the sample set a second time, removing those pulses that are very different from the average, and average the survivors. This method has the advantage of not injecting any information about the pulses which may not be accurate.

To process the signal, we first invert it, then remove any DC offset, then remove the slowly varying component ($f < 200$ kHz), and then run a simple peak detection algorithm to locate pulses. We then compare the shape of the found pulses to that of the average pulse. If both the mean square of the residual and the maximum of the residual are sufficiently small ($< 0.2 V^2$), the pulse is registered.

An additional facet to the algorithm that is important at high count rates is dealing with double hits. These are dealt with in an identical manner to the single pulses. However, because double hits are more rare and because there is more variation in their shape due to differing arrival times, the residual criterion is more lenient ($< 0.4 V^2$).

An example shot (MST shot number 1160926027) without a collimator in front of the detector is shown in Fig. 3. Peak detection found 4766 pulses to be within the amplitude range for single pulses. They were then evaluated by shape,

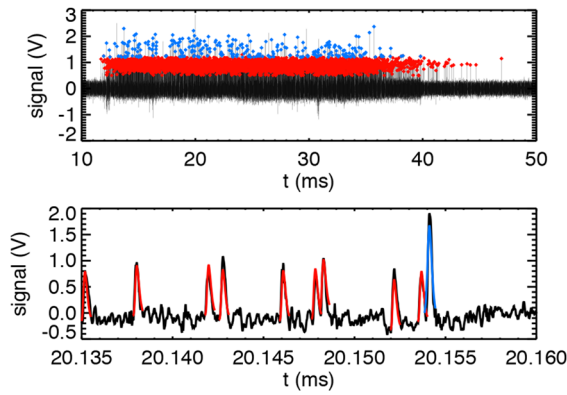


FIG. 3. (Top frame) An example processed signal trace taken without a collimator shows single pulses (red diamonds) and double pulses (blue diamonds). (Bottom frame) A zoomed-in view with ideal pulses overlaid.

and 4541 or 95% were accepted (shown with red diamonds). Peak detection found 284 pulses within the range of double hits, and of those, 276 or 97% survived to be counted (blue diamonds).

Note that the probability of a single hit registering at a given time point is $P = \tau f = 3.3 \times 10^{-3}$, where $\tau = 16.67$ ns is the digitization time and the rate at which pulses arrive is $f \approx 200$ kHz. In the 1.2×10^6 data points recorded during the 20 ms beam-on time, we expect (and obtain) about 4000 single hits. The probability of a double hit is the square of the probability of a single hit times the number of time points of the FWHM of the pulse. From this, we estimate the number of double hits to be about 230, again consistent with the measurement. We are therefore confident that the higher amplitude pulses are truly double hits and not x-rays or some other particles.

IV. PROFILE MEASUREMENTS

A. Orbit tracing

In order to infer the fast ion density profile from the measured fusion emission profile, we must first accurately reconstruct the equilibrium magnetic field so that the 3 MeV proton orbits can be found.

At MST, the magnetic field is reconstructed from all available experimental data using a non-linear Grad-Shafranov solver.¹² The number of fitting free parameters is based on the number and type of available data, and fields are computed on a fine-mesh grid with ~ 1.5 cm spatial resolution. The close-fitting conducting shell carries large image currents to produce the equilibrium vertical field and acts as a flux conserver. The code imposes a perfectly conducting shell boundary condition and up-down symmetry. With the shell image currents balancing the plasma current, the magnetic field falls off rapidly beyond the shell inner surface.

The proton orbits are mapped in reverse in three dimensions to determine the possible loci of the fusion event within the plasma. Outside the machine, a straight line is drawn from the detector position through the collimator to the port-hole. The particle's initial position and velocity upon entering the region of finite magnetic field are used as initial

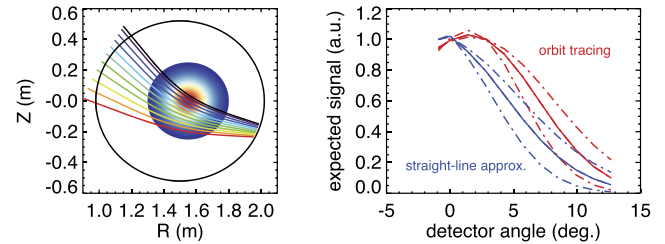


FIG. 4. Proton orbits or, equivalently, detector lines of sight through the plasma (colored lines) found via orbit tracing are plotted over a Shafranov-shifted, Gaussian fast ion density profile with $\sigma = 9$ cm (left). The expected fusion proton signal neglecting (blue lines) and accounting for magnetic deflection (red lines) shows that accurate orbit tracing is critical, even when $\rho_L > a$ (right). The dashed lines represent ± 2 cm bounds on the fast ion density profile.

conditions. The Lorentz acceleration is computed based on the instantaneous velocity and local magnetic field, neglecting any possible E_r (which is small for the energetic proton orbit). The orbit is projected onto the R, Z plane in accordance with the assumption of the toroidal symmetry of the equilibrium.

Figure 4 shows, for each of the 11 experimentally realized collimator aiming angles, the path along which protons in the plasma will reach the detector (colored lines). The contour plot is a Shafranov-shifted, Gaussian density profile with $\sigma = 9$ cm (the Shafranov shift from the equilibrium reconstruction is 5 cm). The corresponding line-integrated signal is calculated and plotted on the right, in red. The dashed-dotted lines represent ± 2 cm bounds on the width of the Gaussian density profile. It can be seen from the range spanned by the dashed-dotted lines that the signal is sensitive to the profile changes of this order. Also plotted in the right frame (in blue) are the expected signals from straight-line trajectories. This is a common approximation when ρ_L , the Larmor radius of the particle, is much larger than the minor radius of the machine, a . Here, although we have $\rho_L \approx 175$ cm and $a = 52$ cm, it is evident that magnetic deflection must be accounted for accurate profile inference.

B. Equilibrium profiles

We measure the equilibrium fusion proton emission profile in 300 kA non-reversed or $F = 0$ plasmas (the reversal parameter F is the ratio of the toroidal magnetic field at the wall to the average toroidal magnetic field). These plasmas are naturally free of the global tearing mode activity which manifest themselves as sawtooth crashes in standard reversed plasmas and are known to redistribute fast ions. This plasma is chosen for the measurement because several ms of quiescent plasma can be averaged over to obtain good counting statistics. The plasmas are also relatively free of x-ray producing fast electrons.

The results are shown in Fig. 5. The time histories of the average count rate from ~ 5 similar discharges for 10 aiming angles are plotted in the left frame. The average profile, found by averaging the count rates in time from $t = 31$ to $t = 35$ ms, is plotted in the right frame with diamonds of corresponding color (consistent with the color code used for the orbits in Fig. 4). The measured proton emission profile is compared to

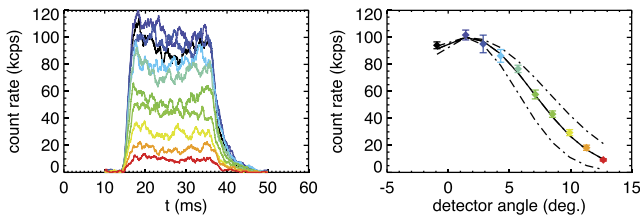


FIG. 5. Equilibrium fast ion density profile measured in non-reversed plasma. Time histories of count rates for each aiming angle (left) and average profile from $t = 31$ to $t = 35$ ms (right) are plotted. The solid black line on the right shows the expected signal profile based on a Shafranov-shifted, Gaussian fast ion density profile with $\sigma = 9$ cm. Bounds of ± 2 cm are shown with the dashed-dotted lines.

a forward modeled signal (black line) found by orbit tracing through a fast ion density profile with $\sigma = 9$ cm and 5 cm Shafranov shift, as described above. The dashed-dotted lines show the effect on the signal of widening or narrowing the fast ion density by 2 cm. This result agrees well with the one obtained from measurements made in similar plasma conditions with a collimated neutron detector. The neutron data predict a Gaussian fast ion density profile with $\sigma = 8$ cm.¹³

C. Dynamic profiles

In order to measure dynamic profiles, we turn to standard reversed plasmas which are punctuated by discrete bursts of magnetic reconnection due to multiple, coupled tearing modes. These sawtooth crashes occur semi-periodically throughout the plasma discharge. To uncover the effect on the fusion emission profile, a large number of similar sawtooth crash events are averaged together (40-50 events per measurement location) by aligning the events in time. To enhance the time resolution of the measurement, the signals from individual shots are added together first and the pulses of the summed signal are counted, rather than counting the pulses first and averaging the count rates, as was done in the $F = 0$ plasmas.

Plotted in the left frame of Fig. 6 are the event-averaged time histories from each measurement location (see Fig. 4 for color code). The time average profile is plotted in the right frame (the time windows for the “before,” “during,” and “after” lines are, respectively, $-0.6 < t < -0.1$, $-0.1 < t < 0.1$, and $0.1 < t < 0.6$ ms). It can be seen that at the time of the crash, the core fast ion density drops by about 30% and the edge increases by a similar amount. The redistribution is fast, happening on time scales of 100 μ s or less.

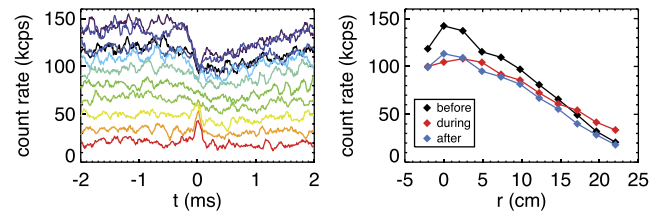


FIG. 6. Dynamic fast ion density profile measured during the course of a global tearing mode burst. The horizontal axis is the impact parameter of the proton orbit to the geometric axis of the machine.

V. SUMMARY

A fusion proton detector has been developed for measuring fast ion profile dynamics. A steerable collimator actuated with a linear feedthrough allows a continuous scanning of the line of sight through the plasma so that the fusion emission profile can be built up over several 10 s of discharges. The fast ion density profile can be reconstructed from the measured emission profile by tracing 3 MeV proton orbits through the reconstructed magnetic field. The results of the measurement indicate that the profile remains constant during non-reversed quiescent plasmas but flattens during global tearing mode activity.

ACKNOWLEDGMENTS

We thank our shareholders for their support and trust and all fellow TAE staff for their dedication, excellent work, and extra efforts. We also thank the MST team for their generous support, ingenuity, and creativity in both the data collection and analysis phases of the project.

¹M. W. Binderbauer *et al.*, *AIP Conf. Proc.* **1721**, 030003 (2016).

²H. Gota *et al.*, *Nucl. Fusion* **57**, 116021 (2017).

³R. M. Magee *et al.*, *Rev. Sci. Instrum.* **87**, 11D815 (2016).

⁴R. M. Magee *et al.*, *Rev. Sci. Instrum.* **85**, 11D851 (2014).

⁵W. W. Heidbrink and J. Strachan, *Rev. Sci. Instrum.* **56**, 501–518 (1985).

⁶R. V. Perez *et al.*, *Rev. Sci. Instrum.* **85**, 11D701 (2014).

⁷J. S. Sarff *et al.*, *Nucl. Fusion* **53**, 104017 (2013).

⁸Passivated Implanted Planar Silicon (PIPS) Detectors, Canberra Industries, Inc., 2012.

⁹E. Specht, see www.packomania.com for information on circle packing theory.

¹⁰J. H. Hubbell and S. M. Seltzer, *Tables of X-ray Mass Attenuation Coefficients and Mass Energy-Absorption Coefficients*. Version 1.4, Report NISTIR-5632 (National Institute of Standards and Technology, 1995), see <http://physics.nist.gov/xaamdi>.

¹¹S. Munaretto, *Phys. Plasmas* **23**, 056104 (2016).

¹²J. K. Anderson *et al.*, *Nucl. Fusion* **44**, 162–171 (2004).

¹³W. J. Capecchi, “A critical fast ion beta in the Madison Symmetric Torus reversed field pinch,” Ph.D. thesis, University of Wisconsin–Madison, 2017.